

Accuracy of Tomo-PIV data for a turbulent round jet

M. Khashehchi¹, C. Atkinson², G.E. Elsinga³, A. Ooi¹, I. Marusic¹ and J. Soria²

¹Department of Mechanical Engineering, University of Melbourne, Melbourne, Victoria, 3010

²Laboratory for Turbulence Research in Aerospace and Combustion, Department of Mechanical and Aerospace Engineering, Monash University, VIC 3800, AUSTRALIA

³Laboratory for Aero and Hydrodynamics, Department of Mechanical Engineering, Delft University of Technology, Delft, THE NETHERLANDS

Abstract

Tomographic-PIV experiment were performed in the far field of an axi-symmetric round jet ($Re_D \approx 3000$) to measure three dimensional velocity fields in a volume of the flow. These 3D data enable the computation of all nine components of the velocity gradient tensor (VGT) at each point in the flow field. The statistical results of Tomo-PIV along the axial direction were assessed by performing a separate set of two-dimensional two-component PIV experiments in a "side-view" plane along the jet axis. This "side-view" plane enabled a comparison between the streamwise and spanwise velocities with the Tomo-PIV results as well as components of turbulence intensities in the streamwise and spanwise directions and Reynolds shear stress.

A study is also conducted to study the consequences of the divergence error in Tomo-PIV. A proposed correction to the divergence error and the implication of this for studying the properties of the VGT are considered.

Introduction

Access to the 3D velocity field can help to understand the dynamics and the physical structures of turbulent flows. Although direct numerical simulations (DNS) has been the main source of good instantaneous 3 dimensional information of the flow, the quality of data obtained from experimental techniques such as particle tracking velocimetry [10], Dual-plane stereoscopic PIV (DSPIV) [8, 5], Holographic particle image velocimetry [11, 15], scalar image velocimetry [14] and tomographic particle image velocimetry (Tomo-PIV) [4] have improved significantly during last two decades. In present study, Tomo-PIV has been performed in the turbulent region of a round jet in order to measure three components of velocity in a volume of the turbulent flow as well as nine components of the velocity gradient tensor. In this method, several simultaneous views of the illuminated particles are used to reconstruct the light intensity distribution by means of optical tomography. 3D cross-correlation of two intensity volumes corresponding to the double frame exposures give three dimensional displacements vectors.

The results are presented from quantitative assessments for the accuracy of velocity gradient component fields obtained from Tomo-PIV measurements in the turbulent round jet. Based on the velocity gradient measurements, divergence error can be analyzed and compared with the DSPIV of Ganapathisubramani et al. (2007), [6]. Furthermore the single point statistics can be compared with the results of the traditional planar PIV measurements, which is the technique of reference in this paper.

Experimental setup

Tomo-PIV has been applied to an axi-symmetric air jet to find the 3D velocity distribution in the self-similar region ($x/d=20$). The separate 2-D planar PIV was designed for the measurement of stream-wise and span-wise components to document the jet

conditions and be used to validate the statistical result of the Tomo-PIV.

Figure 1 shows a schematic diagram of the experimental set-up used in the present research. A test circular nozzle ($D=2\text{mm}$) is mounted on bearings which attach to a rail allowing translation in the vertical plane. The pulsed illumination laser sheet was generated by a double-pulsed Nd:YAG Laser system (BIG Sky Laser). By using a set of optics (cylindrical lens and mirrors), the laser beam was bundled in a planar laser sheet with thickness being about 1mm thick light sheet for planar PIV and 3 mm thick for Tomo-PIV experiments. The time between laser pulses (δt) was 0.01 ms, corresponding to the one quarter law for the in-plane displacement, [2] in the middle of the images. The mean velocity of the flow at the jet outlet was 23 m/s, indicating $Re_d \approx 3000$. The seeding material used is a water-based solution containing 12g/L of sugar. This solution is vaporized by eight Ultrasound devices (APC Nebuliser) which are operated in a cylinder-shape container, with particles that average $2\mu\text{m}$ in diameter. Furthermore, a separate particle generator has been used to seed around the jet to create enough particle density in the shear layer and non-turbulent region. Due to non homogeneity of this type of seeding, each recording start several seconds after seeding to make sure that the background particles are quiescent.

For the Tomo-PIV experiments 4, PCO4000 cameras were used, which were positioned such that all 4 cameras operating in forward scatter with X-95 rails used to mount 2 cameras looking at an angle of 10° down on the jet, while the other 2 cameras look at the same angle upwards towards the jet. All cameras are at an angle of 25° from the angle perpendicular to the direction of the light sheet, (figure 1). The cameras have a spatial resolution of 4008×2670 pixels and a framing rate of 2 HZ in double frame operation position. 200 mm Nikon lenses were fitted to the cameras providing magnification of 0.91, and the field of view of $40 \times 28 \text{ mm}^2$.

All the cameras are operated in double-frame mode and are synchronized with the lasers in order to record the light which is scattered by the tracer particles. Images have been collected at a rate of 2 Hz which corresponds with the maximum frame rate of PCO4000 at double frame mode.

The recorded particle images were analyzed using DaVis software from LaVision GmbH. The 3-D intensity distribution was reconstructed using the MART algorithm with 5 iterations, [4], at a spatial resolution of 100 voxels/mm. The volume frame pairs were interrogated with $44 \times 44 \times 44$ interrogation volume size with 50 percent overlap. Each volume yields $(153 \times 76 \times 22 =) 404000$ velocity vectors with spatial resolution of 0.4 mm.

Turbulent velocity and scalar statistics

Throughout this paper, x , y and z are the stream-wise, span-wise

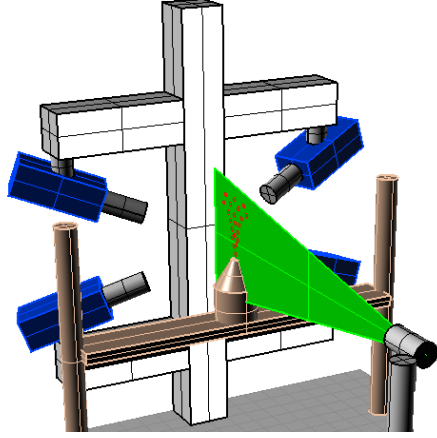


Figure 1: Schematic of the jet experiment setup.

and laser-sheet normal axes, with u , v and w denoting the respective fluctuating velocity components which were calculated by subtracting the total velocity component from the time-averaged component in each direction. The result for the mean centerline velocity U_c , turbulence intensity of stream-wise and span-wise velocity components and Reynolds shear stress, for planar result, $\langle uv \rangle$ are shown in figure 2. In all the graphs, velocity magnitudes are normalized by U_c , which is the maximum centerline of U and the radius is normalized by h where h is the local half-width of U . The Tomo-PIV data are seen to agree reasonably with the planar PIV results with the largest differences appears for the v -RMS statistics. The results are all compared to those of Hussain *et al.* [7], and again good general agreement is observed.

Accuracy assessment

In this section the accuracy of the computed velocity gradient is presented in order to evaluate the effect of the divergence error in the computed results. Following Ganapathisubramani, [6], the quality of the velocity gradient results can be evaluated by comparing certain quantities of the velocity gradient with isotropic conditions. For example, an isotropic condition implies that the following ratios, $\left(\frac{[\delta u / \delta y]^2}{[\delta u / \delta z]^2}\right)$, $\left(\frac{[\delta v / \delta x]^2}{[\delta w / \delta x]^2}\right)$, $\left(\frac{[\delta v / \delta y]^2}{[\delta w / \delta z]^2}\right)$ and $\left(\frac{[\delta v / \delta z]^2}{[\delta w / \delta y]^2}\right)$, should all be equal to 1. The measured values of isotropic ratios for Tomo-PIV results are 0.9312, 1.052, 0.8517 and 0.8312 respectively. These results show at least a 15 percent variation from the isotropic condition. These results are very similar with the result of Ganapathisubramani *et al.* (2007) where the values of ratios indicate approximately 10% deviation from the isotropic condition.

The accuracy of the computed velocity gradients can also be evaluated by measuring the divergence error. If the continuity equation is satisfied, the values of $\nabla \cdot U$ for each data point should be equal to zero. However, due to experimental errors, values of $\nabla \cdot U$ calculated using the Tomo-PIV data is not zero (divergence error in the results). Figure 3 shows the pdf of normalized (relative to the velocity gradient norm) value of $\nabla \cdot U$. This distribution has the mean value of zero and the RMS equal to 0.35, which is very similar to the result of cinematographic stereoscopic PIV by [6] and dual-plane stereoscopic PIV measurements by [12].

Based on the results above, in addition to the intrinsic Tomo-PIV errors (movement of the ghost particles), the noise resulting from computation of velocity gradients have contributed to the errors in the divergence field. In this study, a central differenc-

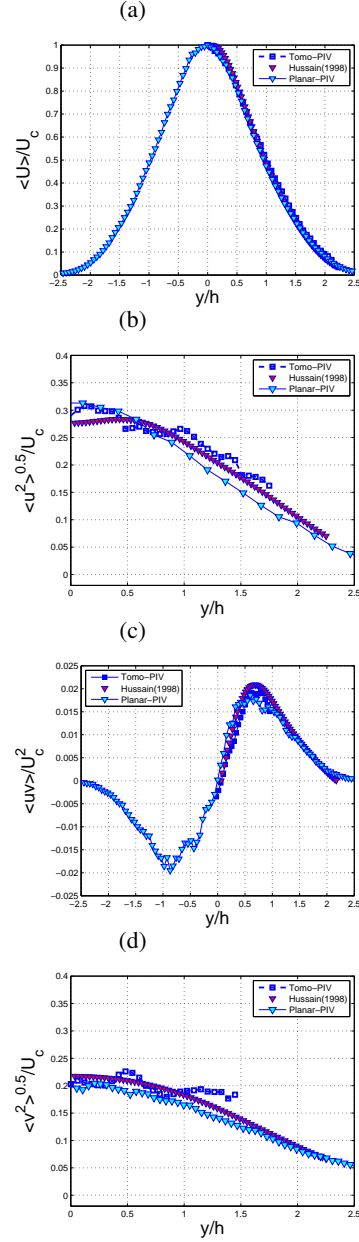


Figure 2: Profiles of several one point statistics at the self-similar region from the present Tomo-piv result compared with the planar PIV and the experimental results from [7]: a – Mean stream-wise velocity profile, b – stream-wise RMS, c – Reynolds shear stress and d – span-wise RMS. U_c is the stream-wise mean centerline velocity and h is the half-width of the jet.

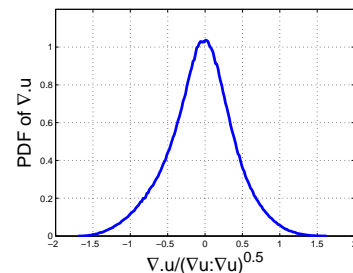


Figure 3: PDF of divergence error relative to the norm of the VGT

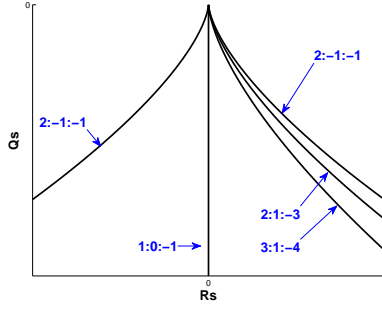


Figure 4: Sketch of the invariant maps of rate of strain tensor. (R_s, Q_s) -space corresponding to different ratios of eigenvalues of rate of strain tensor

ing scheme has been used to calculate all components of VGT. The uncertainty due to computation of velocity gradients can only be reduced by improving the quality of the velocity data. One other way to nominally correct the effect of the error in the divergence field is to force diagonal values of the VGT to be zero. The effect of this proposed correction will be investigated in the following section.

Divergence-free results

The Tomo-PIV data were used to compute the nine components of the velocity gradient tensor (VGT), $A_{ij} = \frac{\partial u_i}{\partial x_j}$, as well as the symmetric part (rate-of-strain) and the skew-symmetric part (rate-of-rotation) of the VGT, $A_{ij} = S_{ij} + W_{ij}$. Three invariants of the VGT can be found by the characteristic equation:

$$\lambda_i^3 + P\lambda_i^2 + Q\lambda_i + R = 0 \quad (1)$$

Since the trace of the rate of strain tensor (S_{ij}) is invariant under rotation and is equal to the dilatation, the sum of the orthogonal components of this tensor should be equal to zero. The deviation from zero can be attributed to the divergence error present in the data due to the errors in measurement of velocity from the Tomo arrangement and the error due to the experimental setup. The distribution of the trace of S_{ij} is identical to the distribution of the divergence error in figure 3 and the RMS value of the distribution is 0.35, which is consistent with the values computed from other works (holographic PIV [15] and dual-plane stereoscopic PIV [12]).

The value of the dilatation can also be measured by the sum of three principal eigenvalues ($\alpha + \beta + \gamma$), where α , β and γ are first, second and third eigenvalues of S_{ij} tensor, respectively. Since S_{ij} is a symmetric matrix, the value of the eigenvalues are all positive and the plot of jpdf of second and third invariants of S_{ij} , (Q_s, R_s) , fall below the discriminant line (Figure 4), $(D_s = 27R_s^2 + 4Q_s^3)$, and tend to be skewed toward the right hand side of the graph ($R_s > 0$) indicating a predominance of sheet structures, [2]. Again if we assume $\alpha > \beta > \gamma$, the different curves in figure 4 corresponds to the ratio of eigenvalues (e.g. 1:1:-2 equal to $\alpha : \beta : \gamma$). The most probable geometry observed in several turbulent flows corresponds to a ratio of 3:1:-4 or 2:1:-3, [1].

One way to remove the effect of the divergence error is to force VGT to be divergence free. A modified value of the velocity gradient tensor is calculated for all points in the flow field

$$A'_{ij} = A_{ij} - \frac{1}{3}\delta_{ij}A_{kk} \quad (2)$$

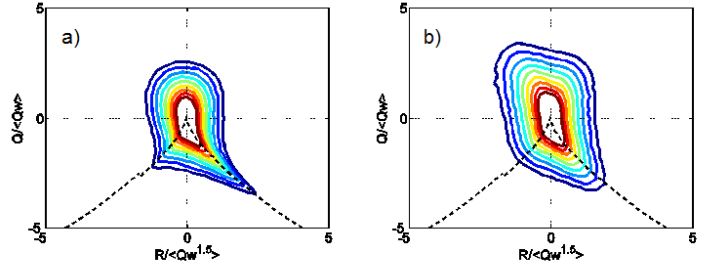


Figure 5: Jpdf of the invariant maps of VGT (R, Q) . a) divergence free results and b) original Tomo-PIV results

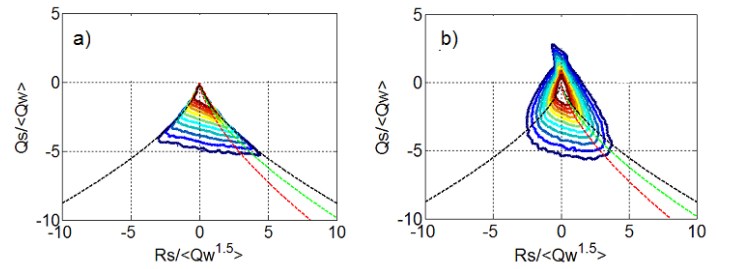


Figure 6: jpdf of the invariant maps of rate of strain tensor (R_s, Q_s) . a) divergence free results and b) original Tomo-PIV results

Then new values of the invariants of VGT can be calculated from A'_{ij} . To see the contribution of the corrected invariant (P) in the result of the topology of the flow, the joint pdf of the second and third invariants of the VGT are computed and presented in normalized form in figure 5a. To make a comparison with the original results the jpdf of R, Q for the original data was also plotted in figure 5b. The invariants are normalized with the $\langle Q_w \rangle$, where $\langle Q_w \rangle$ is taken for the same area as R and Q .

The results reveal a good qualitative agreement with those obtained in the original data, although only a more detailed view of the area in the self-similar region is presented here. Furthermore, except for the tail of the tear-drop, there appears to be a greater asymmetry in the other region for corrected data than the original data in the Q direction.

Figure 6 shows the jpdf of the invariants R_s and Q_s for two of the above mentioned cases. The apparent excursions above the discriminant line which can be seen in figure 6b are the result of the non-zero value of the continuity equation and is corrected in figure 6a. The contour levels shown are the same as those used for the jpdf distributions presented for R and Q plot. As mentioned, the symmetry of S_{ij} forces the data to fall below the discriminant line $D_s = 0$. Deviations above this line are due to noise and error resulting in a non zero divergence for velocity. The color dashed lines in the graph show the regions where the eigenvalues of the rate of strain tensor has the ratio $\alpha : \beta : \gamma$, (black line (1:1:-2), green line (2:1:-3) and red line (3:1:-4)). The graphs may not appear to have any fundamental difference but the average of the eigenvalues of the rate of strain tensor for the two cases show that for the divergence free case the eigenvalues have the ratio 2.2:1:-3.2 and for the original data this ratio is found to be 2.3:1:-3.8. Note that small excursion above the discriminant line causes these differences in the mean eigenvalues. Figure 6 also shows the tendency of the contour lines toward the right hand side of the discriminant line.

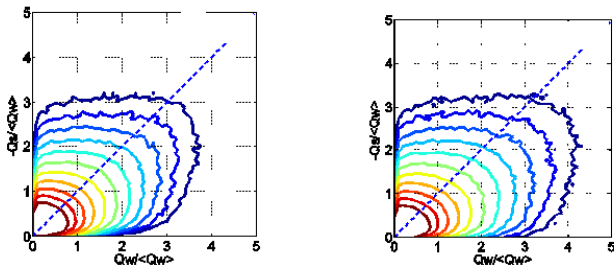


Figure 7: jpdf of the second invariant maps of rate of strain and rate of rotation tensor ($Q_w, -Q_s$). a) divergence free results and b) original Tomo-PIV results

The iso-contour of jpdf of the second invariants of rate of strain and rate of rotation tensors, $-Q_s$ and Q_w respectively, for the original and corrected data are plotted in figure 7. As expected, due to the axi-symmetry nature of the W_{ij} , jpdf does not show any fundamental difference in the Q_w axis, rather slight improvement in the Q_s axis.

The previous graphs show that forcing divergence of the velocity vectors to be equal to zero could be a way for nominally correcting for the small excursion in the invariants plots, specially for the jpdf of the (R, Q) and (Q_w, Q_s) .

Conclusions

An experimental assessment of Tomo-PIV in a turbulent round jet was presented. The velocity distribution in the self-similar region of the jet is measured at a free stream velocity of 23 m/s ($Re \approx 3000$). A four-camera system was used with a maximum angle between the cameras of 25 degrees.

The results of Tomo-PIV data enabled the computation of all nine components of the velocity gradient tensor at each point in a volume. Statistical results of the Tomo-PIV have been validated by performing a separate Planar PIV experiment in the same region of the Tomo-PIV.

The accuracy of the velocity gradients computed from the three dimensional data was investigated by computing the divergence error in the flow field. The RMS of the dilatation error relative to the norm of the velocity gradient tensor was found to be 0.35 and this value is consistent with results in other studies such as [15] and [6, 12].

Probability distributions of the invariants of the VGT and velocity gradients computed using a dilatation correction were almost identical. The jpdf of the direct spatial gradients and the derived spatial gradients were found to be qualitatively similar.

Overall, the Tomo-PIV technique has here been shown as a viable technique for measuring the complete velocity gradient tensor in turbulent round jets, to within a particular uncertainty. The technique allows direct measurement of an instantaneous volume of data that can be utilized to study the structure of vorticity field, strain-rate field and kinetic energy dissipation in turbulent shear flows.

Acknowledgements

The support of the Australian Research Council is gratefully acknowledged.

References

[1] Ashurst, W., Kerstein, A., Kerr, R. and Gibson, C. Alignment of vorticity and scalar gradient with strain rate in sim-

ulated Navier-Stokes turbulence., *Phys. Fluids*. **30**, 1987, 2343.

[2] Blackburn, H., Mansour, N. and Cantwell, B. Topology of fine-scale motions in turbulent channel flow., *J. Fluid Mech* **310**, 1996, 269.

[3] Da-silva, C. B. and Pereira, J. C. F. Invariants of the velocity-gradient, rate-of-strain, and rate-of-rotation tensors across the turbulent/nonturbulent interface in jets., *Phys. Fluids* **20**, 2008, 055101.

[4] Elsinga, G.E. Tomographic particle image velocimetry., *Exp. Fluids*. **41**, 2006, 173–181.

[5] Ganapathisubramani, B., Longmire, E. K., Marusic, I. and Pothos, S. Dual-plane PIV technique to measure complete velocity gradient tensor in a turbulent boundary layer., *Exp. Fluids* **39**, 2005, 222.

[6] Ganapathisubramani, B. and Lakshminarasimhan, K. Determination of complete velocity gradient tensor by using cinematographic stereoscopic PIV in a turbulent jet., *Exp. Fluids* **42**, 2007, 923–939.

[7] Hussain, HJ. A Selection of Test Cases for the Validation of Large-Eddy Simulations of Turbulent Flows., *AGARD ADVISORY REPORT* **345**, 1998.

[8] Kähler, C. J. Investigation of the spatio-temporal flow structure in the buffer region of a turbulent boundary layer by means of multiple plane stereo PIV., *Exp. Fluids* **36**, 2004, 114.

[9] Keane, R. D. and Adrian, R. J., Theory of cross-correlation analysis of PIV images., *Appl. Sci. Res*, **49**, 1992, 191.

[10] Maas, H. G., Gruen, A. and Papantoniou, D., Particle tracking in three dimensional turbulent flows?part I: Photogrammetric determination of particle coordinates ., *Exp. Fluids* **15**, 1993, 133.

[11] Meng, H. and Hussain, F. Instantaneous flow field in an unstable vortex ring measured by HPIV., *Phys. Fluids* **7**, 1995, 9.

[12] Mullin, J. A. and Dahm, WJA. Dual-plane stereo particle image velocimetry measurements of velocity gradient tensor fields in turbulent shear flow. I. Accuracy assessments., *Phys. Fluids* **18**, 2006, 1.

[13] Soria, J., Sondergaard, R., Cantwell, B. , Chong, M. S. and Perry, A. A study of the fine-scale motions of incompressible time-developing mixing layers., *Phys. Fluids A* **6**, 1994, 871.

[14] Su, L. K. and Dahm, WJA. Scalar imaging velocimetry measurements of the velocity gradient tensor field in turbulent flows. II. Experimental results., *Phys. Fluids* **8**, 1996, 507–521.

[15] Zhang, J., Tao, B. and Kats, J. 1997 Turbulent flow measurement in a square duct with hybrid holographic PIV., *Exp. Fluids*. **23**, 1997, 373–381.